ARTICLE

Photocatalytic ethene synthesis from ethane dehydrogenation with high selectivity by ZnO-supported Pt nanoparticles

Wenyu Guo,[a] Wenwen Shi,[a] Junjian Cai,[a] Fen Wei,[a] Xiahui Lin,*[b] Xuefeng Lu,[a] Zhengxin Ding,*[a] Yidong Hou,[a] Guigang Zhang[a] and Sibo Wang*[a]

Thermal catalytic oxidative dehydrogenation of ethane with O_2 is extensively studied as an approach for ethene production, but this approach is energy intensive and bears overoxidation, high-cost and safety concerns. Herein, we present ZnO-supported Pt nanoparticles are highly active and selective for dehydrogenating ethane to ethene by simulated sunlight via a photo-supported Mars-van Krevelen mechanism. The Pt/ZnO catalyst achieves a high ethane-to-ethene conversion rate of 867.8 µmol h^{-1} g^{-1} and an excellent selectivity of 97.56%. Besides, it is also coking-resistant and can be readily revived by exposure to O_2 for refilling the consumed lattice oxygen to preserve its original activity. It is revealed that the Pt species facilitate C_2H_4 desorption from the catalyst to inhibit overoxidation and enhance separation of light-induced charges to boost the photocatalytic efficiency. Whilst the photogenerated holes on ZnO are captured by surface lattice oxygen to generate active $O^{\bullet-}$ species extracting H atoms from adsorbed C_2H_6 to produce C_2H_4. *In-situ* diffuse reflectance infrared Fourier transform spectroscopy is applied to detect the key intermediates and thus propose the possible catalytic EDH process over the Pt/ZnO photocatalyst.

Introduction

As one of the major feedstocks in modern chemical industry, ethene (C_2H_4) is traditionally produced from high-temperature steam cracking of naphtha or ethane.[1-3] Despite being applied industrially for several decades, these steam creaking recipes are extremely energy consumptive and release substantial CO_2, because of the burning of fossil fuels to run the cracking furnaces (> 800 °C).[4-6]

Alternatively, the thermal catalytic ethane dehydrogenation (EDH) with O_2 is extensively studied as a more environmental-friendly method for ethene production.[7,8] Such an oxidative EDH reaction is thermodynamically favourable due to the exothermic nature and can be operated at reduced temperatures (*ca.* 550) to realize an acceptable ethane conversion. In general, metal oxide catalysts can work the oxidation reaction via a Mars–van Krevelen mechanism, which involves the oxidation of gas-phase reactants by the surface-active lattice oxygen ($O_{latt.}$), leading to the formation of oxygen vacancies ($O_{vac.}$). Subsequently, the generated $O_{vac.}$ can be replenished by the activated molecular O_2 to complete the catalytic cycle. Nonetheless, this EDH technique requires cofeeding of ethane and O_2, which imposes safety concerns resulted from the flammability of the mixed gases as well as

increases the costs for on-site O_2 generation and product purification. Also, the overoxidation of ethene product to valueless CO_2 is usually engaged, reducing the selectivity of ethene.[9]

In recent years, the selective dehydrogenation of alkanes to alkene has been shown by several groups using semiconductive catalysts by light,[10-17] activating the enormous potential of photocatalysis for making ethene from ethane, which holds the distinct benefits of breaking thermodynamic limitations and driving the reaction under mild conditions. For instance, Yue and coworkers have demonstrated photocatalytic EDH to produce C_2H_4 by a TiO_2-supported Cu catalyst under UV light irradiation at room temperature, attaining a C_2H_4 productivity of 533.46 µmol h^{-1} g^{-1} and a C_2H_4 selectivity of 98.4%.[18] Very recently, we have found that a $LaVO_4$ catalyst enables EDH by simulated sunlight via dynamic cooperation between $O_{latt.}$ and $O_{vac.}$, which shows a C_2H_4 yield of 15.4 µmol h^{-1} g^{-1} and a C_2H_4 selectivity of 47.8%.[19] Further, the preliminary results indicate that loading Pt on the $LaVO_4$ surface can drastically improve C_2H_4 production and selectivity to 275 µmol h^{-1} g^{-1} and 96.8%; however, the working functions of Pt in the EDH reaction require detailed exploitation. These works inspire that the efficient and selective light-driven ethene production may be succeeded from EDH by Pt species supported on suitable metal oxide catalysts.

Herein, a Pt/ZnO hybrid photocatalyst is prepared by loading Pt nanoparticles on the surface of commercialized ZnO through an impregnation-reduction method, which exhibits a superior performance for EDH to generate C_2H_4 via a light-enhanced Mars-van Krevelen (MvK) mechanism.[20,21] The Pt/ZnO catalyst

[a] State Key Laboratory of Photocatalysis on Energy and Environment, College of Chemistry, Fuzhou University, Fuzhou 350116, P. R. China
[b] College of Environment and Safety Engineering, Fuzhou University, Fuzhou, 350108, P. R. China

accomplishes a high ethane-to-ethene conversion rate of 867.8 μmol h^{-1} g^{-1} and a selectivity of 97.56%. Also, it displays a fine anti-carbon deposition ability and can be readily restored by exposure to O_2 for replenishing the consumed lattice oxygen ($O_{latt.}$) to realize a simplistic regeneration to recuperate the pristine reactivity. The Pt species is proved to accelerate C_2H_4 desorption from the catalyst to prevent overoxidation as well as to improve separation of light-induced charges to reinforce the photocatalytic efficiency. Whilst the photo-induced holes are captured by the surface $O_{latt.}$ of ZnO, which facilitates the creation of reactive $O^{\bullet-}$ species to extract H atoms from adsorbed C_2H_6 to produce C_2H_4. The possible photocatalytic EDH mechanism is proposed, based on the key reaction intermediates determined by *in-situ* diffuse reflectance infrared Fourier transform spectroscopy (DRIFTS).

Experimental section

Synthesis of catalysts

The ZnO-supported Pt nanoparticle catalysts were prepared by a classic impregnation-reduction method. Typically, 300 mg of commercial ZnO powder was added to 15 mL of H_2O containing a certain amount of $H_2PtCl_6 \cdot 6H_2O$ solution (10 mg Pt mL^{-1}, varying from 0.2 to 2 wt%) under stirring for 10 min. After sonication for 20 min, the resultant mixture was transferred into an oil bath at 107 °C under continuously stirring until the solvent was evaporated completely to collect the solid powder precursor. The x%Pt/ZnO (x = 0, 0.2, 0.5, 1.0 and 2.0) catalysts were obtained by annealing the precursor in a 5%H_2/Ar flow (150 mL min^{-1}) at 500 °C for 1 h with a heating rate of 10 °C min^{-1}. Unless stated otherwise, the catalysts selected for all the studies were the 1.0%Pt/ZnO sample, which was shortened hereafter as Pt/ZnO for clarity.

Photocatalytic EDH performance evaluation

The photocatalytic EDH reaction was conducted in a customized glass-closed reactor (150 mL in volume) equipped with a quartz window on the top to harvest photo irradiation using a 300 W Xe lamp as the light source. In the typical reaction, a mixture of 50 mg of catalyst and 1 mL of H_2O was dispersed uniformly on a quartz substrate, followed by heating at 100 °C for 20 min to get a catalyst thin film, which was then placed in the middle of the reactor and vacuumed to get an anaerobic environment. Afterward, the mixed gas of C_2H_6 and Ar (Ar：C_2H_6 = 9:1) was introduced with a partial pressure of 1 atm to start the reaction. After each reaction, the hydrocarbons (i.e., C_2H_6, C_2H_4, and CH_4) in the reactor were quantified by a An Agilent 7890B gas chromatograph (GC) equipped with a HP-PLOT/Q column and a flame ionization detector (FID), and the produced H_2 and CO were quantified by a GC equipped with a thermal conductivity detector (TCD) and methanizer-coupled FID.

Results and discussion

The ZnO powder was blended with the $H_2PtCl_6 \cdot 6H_2O$ solution through an impregnation approach to load the Pt precursor

(i.e., $[PtCl_6]^{2-}$) on the surface. The Zeta potential tests indicate that ZnO dispersed in H_2O holds the positive potential and the platinum species are negatively charged (Fig. S1, ESI), which allows them to assemble spontaneously by an electrostatic interaction with the Pt precursor adsorbed on the ZnO surface.[22,23] Afterward, the loaded Pt species were reduced by a 5%H_2/Ar flow to achieve Pt/ZnO catalyst. By regulating the added mass of $H_2PtCl_6 \cdot 6H_2O$, four samples, namely, 0.2%Pt/ZnO, 0.5%Pt/ZnO, 1.0%Pt/ZnO and 2.0%Pt/ZnO were prepared (the percentage denotes the calculated weight of Pt), respectively. Inductively coupled plasma optical emission spectrometry (ICP-OES) confirms the actual Pt contents of these x%Pt/ZnO samples (Table S1, ESI), which are close to the theoretical values.
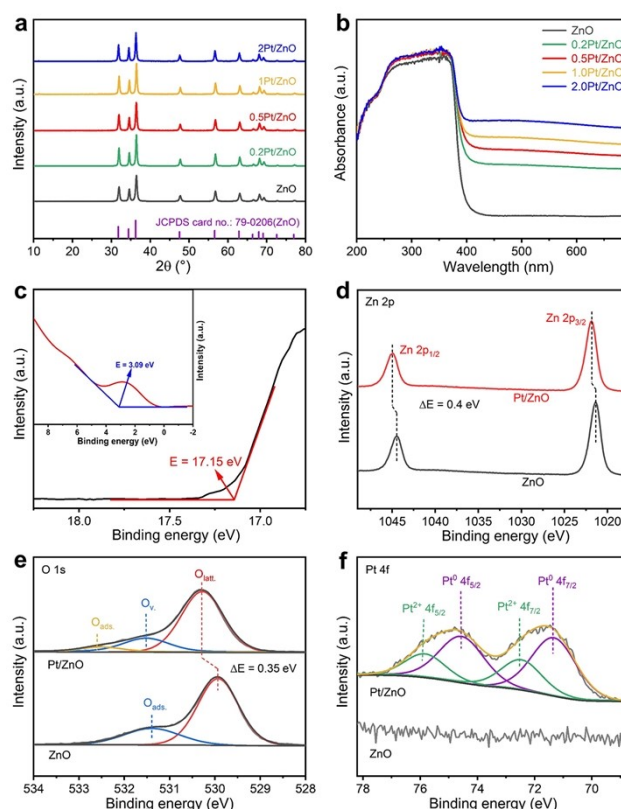
Fig. 1 (a) XRD patterns (b) DRS spectra of ZnO and Pt/ZnO samples. (c) UPS spectrum of ZnO. (d) Zn 2p spectra, (e) O 1s spectra and (f) Pt 4f spectra of ZnO and Pt/ZnO.

Crystal structures of the x%Pt/ZnO catalysts were studied by powder X-ray diffraction (XRD). As shown in Fig. 1a, all the diffraction peaks are correspondingly assigned to the hexagonal wurtzite phase of ZnO (JCPDS card no. 79-0206).[24,25] Meanwhile, the positions and intensities of the diffraction peaks of Pt/ZnO remain almost unchanged compared with that of pure ZnO, implying that the Pt species are loaded on the surface of ZnO, rather than incorporated into the lattice.[25] Noteworthily, no obvious signal attributable to Pt nanoparticles is detected in the XRD patterns of Pt/ZnO, which indicates the formation of highly dispersive Pt particles with ultrasmall size.[23,26] The Raman spectrum of ZnO excited by a laser line at 325 nm displays three characteristic bands of the wurtzite

phase centred at 572, 1145 and 1725 cm^{-1} (Fig. S2, ESI), which result primarily from the polar symmetry modes A_1(LO) and the overtones.[27,28] No noticeable alternation is observed over the Raman of ZnO after modified with the Pt species, further emphasizing the high crystal structure stability of the ZnO support against the Pt-loading process.

UV-Vis diffuse reflection spectroscopy (DRS) was used to explore the optical properties of ZnO and Pt/ZnO samples. As shown in Fig. 1b, pure ZnO exists a strong absorption in the ultraviolet region with the edge at ca. 380 nm, in agreement with its wide band-gap feature.[29,30] Whilst all the Pt/ZnO composites display enhanced absorption in the visible region, which is interpreted by the interband transition of non-plasmonic Pt metal.[31] The band gap energy (E_g) of ZnO is calculated to be 3.2eV by the Tauc plot (Fig.S3, ESI). The ultraviolet photoelectron spectroscopy (UPS) test confirms the Fermi level (E_f) of ZnO at about -0.78 V (vs. normal hydrogen electrode, NHE, pH = 7, Fig. 1c), which permits determination of its valance band (VB) position at 2.31 V (vs. NHE, pH = 7). And consequently, its conduction band (CB) position is defined at -0.89 V (vs. NHE, pH = 7) by taking the bandgap energy into calculation. Therefore, the band structure of ZnO is specified (Fig. S4, ESI). The E_f of Pt is counted to be 1.25V (vs. NHE, pH = 7). After contact, the Fermi level difference between Pt and ZnO drives electron flow from ZnO to Pt, leading to alignment in their Fermi levels.[32]

X-ray photoelectron spectroscopy (XPS) analysis was performed to examine the surface composition and chemical states of ZnO and Pt/ZnO. The survey spectrum of Pt/ZnO confirms its elemental composition of Pt, Zn and O without the detection of impurity element (Fig. S5a, ESI), which is reaffirmed by the energy dispersion spectrum (EDS, Fig. S5b, ESI). In the Zn 2p XPS spectrum of ZnO (Fig. 1d), the binding energies of Zn $2p_{3/2}$ and Zn $2p_{1/2}$ peaks are 1021.40 and 1044.50 eV with an energy interval of ~23 eV, confirming the appearance of Zn^{2+} lattice cations.[16,33-35] The O1s spectrum of ZnO is fitted into two peaks located at 529.93 and 531.35 eV (Fig. 1e), attributing to the $O_{latt.}$ of ZnO and the surface adsorbed oxygen species ($O_{ads.}$), respectively.[16,36] In comparison, the O1s spectrum of Pt/ZnO is divided into three peaks with the dominant one positioned at 530.28 eV, corresponding to the $O_{latt.}$, as well as additional two peaks at 531.52 and 532.50 eV that are assigned to the surface $O_{v.}$ and $O_{ads.}$, respectively.[19] The formation of $O_{v.}$ is resulted from the hydrogen reduction treatment involved in the Pt/ZnO synthesis process. The electron paramagnetic resonance (EPR) analysis further validates the existence of $O_{v.}$ in Pt/ZnO (Fig. S6, ESI). It is further observed that, the binding energies of Zn 2p and $O_{latt.}$ of Pt/ZnO are both shifted toward the positive values, compared with those of pure ZnO. These results indicate the strong interaction between Pt and ZnO.[11] The Pt 4f XPS spectrum of Pt/ZnO reveal that the Pt $4f_{7/2}$ and Pt $4f_{5/2}$ peaks are deconvoluted into two spin-orbit doublets (Fig. 1f), ascribing to the dominant population of Pt^0 and the minor proportion of Pt^{2+}.[26,37] To be specific, the peaks with binding energies of 71.32 and 74.56 eV correspond to Pt $4f_{7/2}$ and Pt $4f_{5/2}$ of metallic Pt, while those at 72.47 and 75.83 eV are assigned to Pt $4f_{7/2}$ and Pt $4f_{5/2}$ of Pt^{2+}, respectively.

Morphologies of the samples were characterized by field emission scanning electron microscopy (FESEM) and transmission electron microscopy (TEM). Pristine ZnO holds an irregular morphology of nanoparticles in size around 20-40 nm (Fig. S7, ESI). No obvious change in the morphology is monitored after ZnO is loaded with the Pt species (Fig. 2a). The TEM image of Pt/ZnO validates its nanoparticulate shape (Fig. 2b), and numerous tiny Pt particles (indicated by yellow circles) are discerned on the surface of ZnO particles. A closer TEM analysis determines the average size of the Pt nanoparticles of ca. 2.6 ± 0.13 nm (Fig. 2c). The presence of the Pt nanoparticles is evidently shown by the magnified TEM image (Fig. 2d). In the high-resolution TEM (HRTEM) image (Fig. 2e and Fig. S8, ESI), the well-resolved lattice fringes with interlayer spacings of 0.248 and 0.22 nm are indexed to the (101) and (111) crystal planes of ZnO and Pt, respectively.[26,38] This signifies the intimate contact between ZnO and Pt, which is conducive to facilitate the separation of photoexcited chares. The elemental mapping analysis exposes the relatively homogeneous distribution of Zn, O and Pt elements in Pt/ZnO (Fig. 2f).
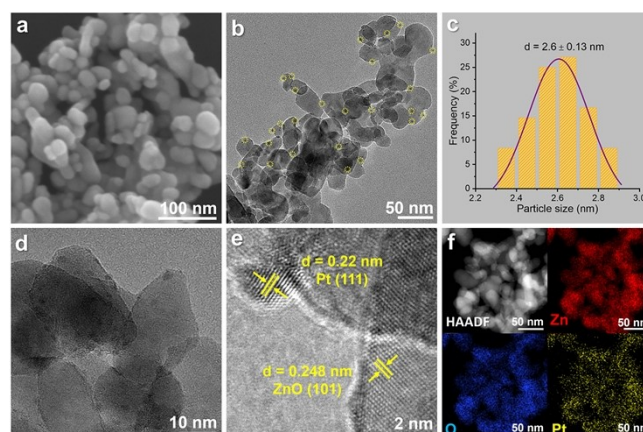

Fig. 2 (a) FESEM image and (b) TEM image of Pt/ZnO. (c) Particle size distribution diagram of Pt in Pt/ZnO. (d) TEM image, (e) HRTEM image, and (f) HAADF and the corresponding elemental maps of Pt/ZnO.

Photocatalytic EDH performance of ZnO and Pt/ZnO samples were assessed by a gas-solid phase reaction with simulated sunlight. As shown in Fig. 3a, pristine ZnO is inactive to the EDH reaction. Strikingly, after loading Pt nanoparticles as a cocatalyst, all the x%Pt/ZnO (x = 0.2, 0.5, 1, 2) catalysts display remarkably improved EDH activity, producing C_2H_4 and H_2 as the main products, coupled with a small generation of CH_4 and CO. Of note, the 1% Pt/ZnO (i.e., Pt/ZnO) sample achieves the optimal performance, affording C_2H_4 and H_2 at rates of 867.8 and 886.4 µmol $h^{-1} g^{-1}$, respectively, which corresponds to a high C_2H_4 selectivity of 97.56% and a C_2H_6 conversion of 6.4%. The C_2H_6-to-C_2H_4 evolution rate is among the state-of-the-art values under comparable conditions (Table S2). It should be pointed out that, when the Pt loading mass is higher than 1wt%, Pt/ZnO catalyst shows a lowered photocatalytic EDH activity, which might be caused by excessive Pt nanoparticles covering the catalytic-active sites and promoting charge carrier recombination.[26] In addition, the photocatalytic EDH activities of ZnO deposited with other metals (i.e., Pd, and Au) were also

evaluated under otherwise identical conditions (Fig. S9, ESI). Pd/ZnO manifests only the half activity that of Pt/ZnO, and Au/ZnO is almost inactive to the EDH reaction. Such results underline the crucial role of Pt to the dehydrogenative conversion catalysis, probably due to the catalytic function of Pt in activating the C-H bond and reducing the dissociated H atoms.

The time-dependent EDH activity of Pt/ZnO photocatalyst was carried out (Fig. S10, ESI). The production of C_2H_4 and H_2 increases progressively within the first one-hour reaction, accompanied by a small formation of CH_4 and CO. Afterward, the yield of C_2H_4 tends to be stable with the reaction time, yet the H_2 production still increases together with improvements in CH_4 and CO. This finding points to the increased overoxidation of C_2H_4, owing to its accumulation on the catalyst surface in the batch reactor, which inspires us to operate the photocatalytic EDH reaction in a continuous flow system, and the related study is ongoing in our laboratory.
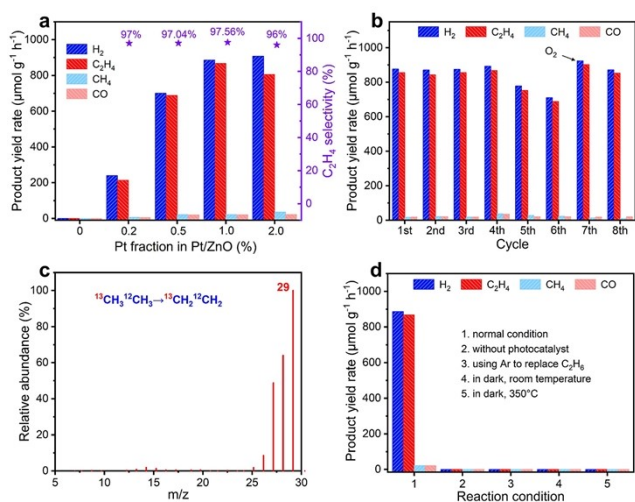
Fig. 3 Photocatalytic dehydrogenation of ethane performance of (a) different fractions of Pt-supported ZnO, (b) activity cyclic tests of Pt/ZnO after regeneration. (c) C_2H_4 produced from the $^{13}CH_3^{12}CH_3$ isotope experiment. (d) Activities under varied reaction conditions. Reaction condition: Ar: C_2H_6 = 9: 1, 50 mg of catalyst.

The fact that CO generates from the photocatalytic EDH reaction without employing a molecular O_2 infers participation of the $O_{latt.}$ of Pt/ZnO through the a MvK mechanism.[19] To check this, the used Pt/ZnO photocatalyst was characterized by EPR. An enhanced signal of $O_{vac.}$ (g = 2.003) is detected (Fig. S11, ESI), compared with that of fresh Pt/ZnO, indicating the consumption of $O_{latt.}$ in the EDH reaction. Moreover, the participation of $O_{latt.}$ is also reflected by activity stability tests of Pt/ZnO (Fig. 3b), demonstrating decreased activities in the 5th and 6th cycles, due to the expenses of surface catalytic-active $O_{latt.}$ and formation of excessive $O_{vac.}$. To replenish the consumed $O_{latt.}$, the used Pt/ZnO catalyst after reacting for 6 cycles was exposed to molecular O_2 for 2h and then further applied to run the EDH reaction. As can been seen from Fig. 3b, the catalyst well restores to the initial reactivity in the 7th and 8th cycles, which is accompanied by its colour returning to almost identical to that of the fresh one (Fig. S12, ESI). This means that the used Pt/ZnO catalyst can realizes a facile regeneration by contact

with O_2. More specifically, the consumed $O_{latt.}$ of Pt/ZnO can be refilled by the molecular O_2 to achieve a chemical cycle, thus preserving the intrinsic catalytic function. During the stability cycling tests, the total generation of C_2H_4 reaches 6616.4 µmol, which delivers a turnover number (TON) of 2232 relative to the active Pt species, determined by ICP-OES and carbon monoxide pulse analysis (Fig. S13, ESI), revealing the catalytic nature of the EDH reaction.

After the activity cycling tests, the used sample was researched by FESEM, XRD and XPS (Fig. S14-16, ESI), and no change is detected in the morphological, crystal and surface structures, which indicates the high stability and fine reusability of the Pt/ZnO photocatalyst. Meanwhile, Raman and thermo-gravimetric analyses uncover that nearly no carbon deposition forms on spent Pt/ZnO catalyst (Fig. S17, ESI), suggesting the superiority of photocatalytic EDH recipe in anti-coking, which also supports the virtually 100% carbon balance of the reaction.

The ^{13}C-labelled experiment was performed to track the origin of C_2H_4, by using $^{13}CH_3^{12}CH_3$ as the feedstock, and the produced gases were analysed by gas chromatography-mass spectrometer (GC-MS). As shown in Fig. 3c, the MS spectrum indicates that the generated ethene exhibits the dominated signal with a m/z value of 29, corresponding to $^{13}CH_2^{12}CH_2$. In comparison, when utilizing $^{12}CH_3^{12}CH_3$ as the reactant, the dominated m/z signal locates at the value of 28 (Fig. S18, ESI). These results solidly confirm that C_2H_4 product originates from the dehydrogenative conversion of C_2H_6 feedstock.

A series of control experiments were conducted to explore the function of each component in the photocatalytic EDH system. As depicted in Fig. 3d, no product yields when the system is absent with Pt/ZnO, C_2H_6, or light (column 2-4, Fig. 3d), suggesting that the EDH reaction proceeds photocatalytically by Pt/ZnO catalyst. The thermographic technique determines that the surface temperature of the catalyst is about 340 °C during the reaction (Fig. S19, ESI). However, the control experiment authorizes no product creates when the system is manipulated at 350 °C in dark. This outcome highlights that the outstanding EDH performance of Pt/ZnO derives from the photocatalysis effect. Despite this, the relatively high temperature should be beneficial to facilitate mass/charge transfer and product desorption to promote the EDH reaction.

To gain some insights into the source of the excellent EDH performance of Pt/ZnO photocatalyst, the specific surface area and textural properties of the samples were investigated by N_2 adsorption-desorption measurements. Both ZnO and Pt/ZnO exhibit the type-IV N_2 sorption isotherms with H1 hysteresis loop (Fig. S20, ESI), confirming the existence of mesoporous in these materials.[39] The two samples hold almost the same specific surface area, that is, 22 $m^2 g^{-1}$ for ZnO and 23 $m^2 g^{-1}$ for Pt/ZnO. The pore size distribution plots estimate that the average pore width is 26 nm for ZnO and 34 nm for Pt/ZnO, respectively. All these findings reflect the mesoporous structure of ZnO and Pt/ZnO, which is conducive to facilitate C_2H_6 adsorption/activation and mass transport.[40]

Strong metal-support interaction (SMSI) is a representative effect determining the performance of supported catalysts.[41-44]

In our study, the efficiency of photocatalytic EDH is expected to be influenced by the interaction between Pt species and ZnO support. To reveal the SMSI effect of the ZnO-supported Pt photocatalyst as well as to search the desorption behaviours of C_2H_4 and H_2 on the catalysts, temperature-programmed desorption of ethylene (C_2H_4-TPD) and hydrogen (H_2-TPD) tests were performed. The C_2H_4-TPD profiles reveal that Pt/ZnO appears an SMSI effect in comparison with pristine ZnO and the desorption of C_2H_4 shifts obviously to the lower temperatures (Fig. 4a). Specifically, the C_2H_4-TPD profile of pristine ZnO presents two legible peaks cantered at 291 and 418 °C, which are assigned to the continuous desorption of the weakly π-adsorbed C_2H_4 without decomposition and the desorption of C_2-fragments decomposed from the strongly σ-bonded C_2H_4.[45-47] In contrast, the C_2H_4-TPD profile of Pt/ZnO only shows the weakly π-adsorbed ethylene, indicating that the loading of Pt cocatalyst on ZnO facilitates ethylene desorption, which is desirable to avoid overoxidation during EDH reaction.
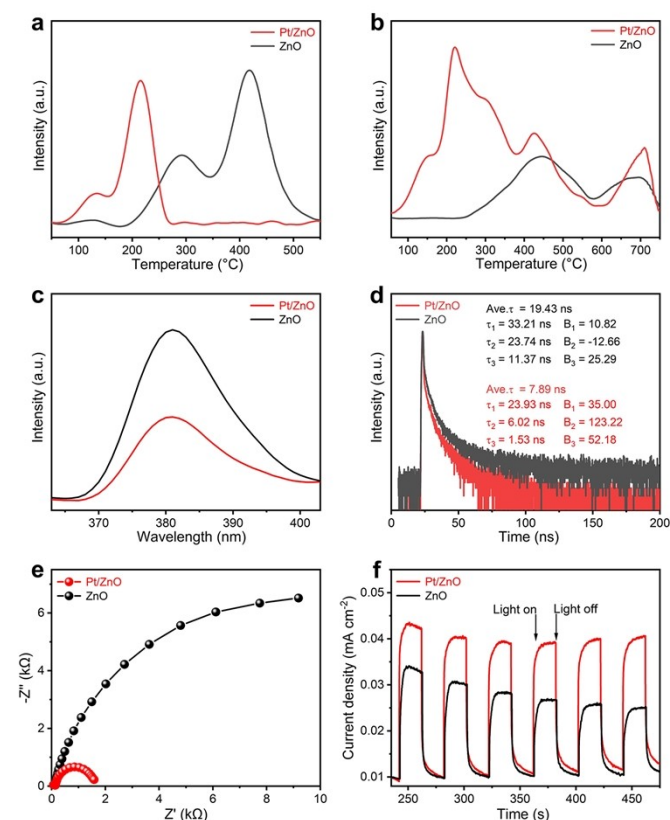

Fig. 4 (a) C_2H_4-TPD, (b) H_2-TPD and (c) Steady-state PL spectra, (d) time-resolved transient PL spectra, (c) EIS Nyquist plots and (d) transient photocurrent responses of ZnO and Pt/ZnO.

On the other side, the H_2-TPD profiles further unveil the SMSI effect of the Pt/ZnO catalyst (Fig. 4b). The H_2-TPD profile of Pt/ZnO demonstrates three distinctive peaks below 400 °C. The peak at about 150 °C corresponds to H_2 desorption on Pt metal, while the rest two peaks at 222 and 305 °C are ascribed to hydrogen spillover on ZnO.[26,48,49] However, the H_2-TPD profile of ZnO displays two broad desorption peaks cantered at around 443 and 695 °C, which are attributed to H_2 desorption from ZnO.

These results manifest that the Pt sites are responsible for H_2 dissociation and the spillover of atomic hydrogen, and thus contributing to the EDH reaction.

A series of photo-/electro-chemical characterizations were utilized to study the dynamic behaviours of photogenerated carriers. The steady-state photoluminescence (PL) spectra reveal that Pt/ZnO renders a decreased PL emission than bare ZnO (Fig. 4c), which suggests that recombination of the charge carriers on Pt/ZnO is inhibited, originating from the effective electron transfer from ZnO to Pt.[50-52] Besides, the time-resolved PL (TRPL) spectra indicate that the decay kinetics of Pt/ZnO exhibits a shorter PL lifetime than that of ZnO (Fig. 4d), reflecting the faster separation of photoinduced electrons and holes in Pt/ZnO.[53-56] Further, the electrochemical impedance spectra (EIS) verify Pt/ZnO possesses a smaller high-frequency semicircle in the Nyquist plot than pure ZnO (Fig. 4e), signifying the lower electronic resistance of Pt/ZnO, which is beneficial to boost separation and transport of the charge carriers in photo-catalysis.[40,57,58] Consistently, the accelerated charge transport of Pt/ZnO is also reflected by the improved photocurrent response in transient photocurrent generation (Fig. 4f).[59 60,61] The above outcomes authenticate that Pt/ZnO empowers improved separation and migration of photoinduced charge carriers, and therefore enabling the superior photocatalytic performance.
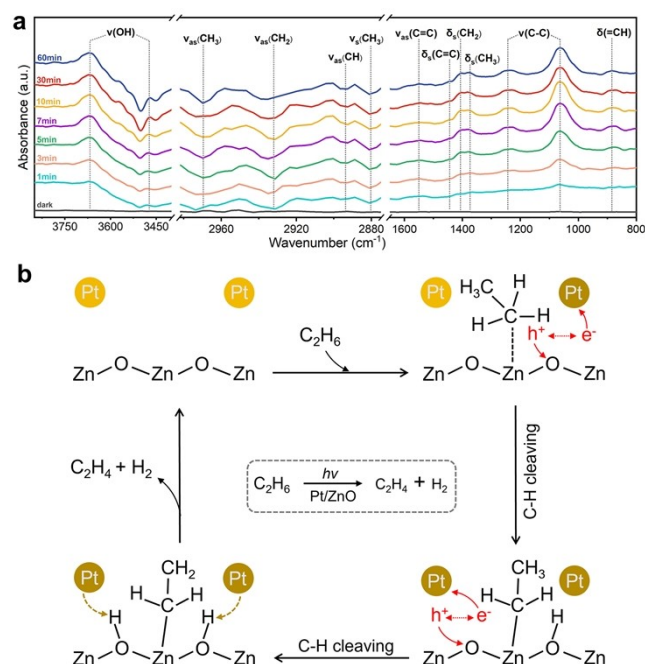
Fig. 5 (a) *In-situ* DRIFTS spectra of photocatalytic dehydrogenation of ethane over Pt/ZnO under light irradiation. (b) The schematic diagram of the proposed photocatalytic dehydrogenation of ethane reaction mechanism about main reaction route over Pt/ZnO.

To elucidate the photocatalytic EDH mechanism, *in-situ* DRIFTS was employed to identify the key intermediates involved in the reaction. The DRIFTS spectra captured in the dark manifests five evident peaks attributable to the stretching vibrations of C-H bonds, which mirrors efficient C_2H_6 adsorption by Pt/ZnO catalyst (Fig. S21, Table S3, ESI).[19] After being

ARTICLE **Journal Name**

irradiation with light, the corresponding peaks at 2880-2980 cm^{-1} become negative (Fig. 5a), suggesting that the absorbed C_2H_6 molecules are consumed for reaction. Alongside, signals of several new species are detected, and their signal intensities are increasingly intensified according to the irradiation time. The bands at 3668 and 3473 cm^{-1} are allocated to the OH stretching vibration,[23,62] which indicates the existence of surface-adsorbed hydroxyl groups (*OH) that can be generated from the coupling of H atom dissociated from ethane with surface active $O_{latt.}$ of ZnO.[10] Importantly, the vibrations of C-H (1408 cm^{-1}), CH_3 (1375 cm^{-1}) and C-C (1243 cm^{-1}) bonds suggest the formation of the key intermediates of CH_3-CH_2• and •CH_2-CH_2•, indicating C-H cleaving of the absorbed C_2H_6.[15,19,63] These results illustrate the dissociation adsorption of C_2H_6 on the surface of Pt/ZnO. In addition, two new bands emerged at 1446 and 1552 cm^{-1}, which are indexed to the bending and stretching vibrations of the C=C bond, respectively.[11,18,64] These two new bands plus the band at 884 cm^{-1} (=CH) jointly confirm the formation of C_2H_6. Such *in-situ* spectroscopic results uncover the key processes of the adsorption and dehydrogenation of C_2H_6 to C_2H_4 over the Pt/ZnO photocatalyst.

The probable photocatalytic EDH mechanism over the Pt/ZnO catalyst is finally proposed, as illustrated in Fig. 5b. Initially, the C_2H_6 molecule is preferentially adsorbed on the surface Zn site of ZnO via its C atom. Upon light irradiation, the electron (e^-) and hole (h^+) are generated in ZnO semiconductor. Then, the photoexcited holes are trapped by surface $O_{latt.}$ to form the catalytic-active $O\bullet^-$ species, which enables C-H cleaving of the adsorbed C_2H_6, leading to the formation of •C_2H_5 and •H species.[10] Afterward, •H is thermodynamically favoured to combine with adjacent $O_{latt.}$ on ZnO surface to generate OH groups. The C-H and •C_2H_5 moieties can further dehydrogenate by the photogenerated holes and desorb from the catalyst surface to form gaseous C_2H_4 and H_2. Concurrently, the Pt particles are effective to capture the photogenerated electrons to promote separation and inhibit recombination of the charge carriers, and consequently, the Pt cocatalyst with collected electrons can effectively promote the reduction of H atom to release H_2. It is noted that a small fraction of adsorbed C_2H_4 encounters minor overoxidation to produce CO at the spend of $O_{latt.}$ (Fig. S22, ESI), which can be replenished with molecular O_2, achieving the regeneration of Pt/ZnO catalyst to maintain the intrinsic EDH activity.

Conclusions

In summary, by supporting Pt nanoparticles on the surface of ZnO, an efficient Pt/ZnO hybrid catalyst is constructed, which shows high productivity and selectivity for photocatalytic ethane dehydrogenation for ethene generation. Under simulated sunlight irradiation, the optimized Pt/ZnO catalyst actively dehydrogenates ethane via a photo-assisted Mars-van Krevelen mechanism, delivering a high ethene yield of 867.8 $\mu mol\ h^{-1}\ g^{-1}$ and an excellent selectivity of 97.56%. Also, the Pt/ZnO catalyst displays a superior coking-resistant property and achieves fine reusability after a facile regeneration by contacting with molecular O_2 to replenish the consumed lattice

oxygen. The Pt species not only promote C_2H_4 and H_2 desorption from the catalyst to inhibit overoxidation but also facilitate charge carrier separation and transport to improve the reaction efficiency. This work may attract wide interest in semiconductor photocatalysis for selective alkane-to-alkene transformation by renewable solar energy under mild conditions.

Author contributions

Wenyu Guo: conceptualization, methodology, validation, writing-original draft, writing-review& editing. Wenwen Shi: methodology, feasibility analysis, validation. Junjian Cai: methodology, validation. Fen Wei: conceptualization, methodology, feasibility analysis. Xiahui Lin: writing-review & editing, supervision, funding acquisition. Xuefeng Lu: writing-review & editing. Zhengxin Ding: writing-review & editing, supervision, funding acquisition. Yidong Hou: writing-review & editing. Guigang Zhang: writing-review & editing. Sibo Wang: conceptualization, feasibility analysis, validation, writing-review& editing, supervision, funding acquisition.

Conflicts of interest

There are no conflicts of interest to declare.

Acknowledgements

Notes and references

1. Y. Gao, L. Neal, D. Ding, W. Wu, C. Baroi, A. M. Gaffney and F. Li, *ACS Catal.,* 2019, **9**, 8592-8621.
2. T. Ren, M. Patel and K. Blok, *Energy,* 2006, **31**, 425-451.
3. H. Saito and Y. Sekine, *RSC Adv.,* 2020, **10**, 21427-21453.
4. Z. Maeno, S. Yasumura, X. Wu, M. Huang, C. Liu, T. Toyao and K.-i. Shimizu, *J. Am. Chem. Soc.,* 2020, **142**, 4820-4832.
5. J. Liu, N. He, Z. Zhang, J. Yang, X. Jiang, Z. Zhang, J. Su, M. Shu, R. Si, G. Xiong, H.-b. Xie and G. Vilé, *ACS Catal.,* 2021, **11**, 2819-2830.
6. M. Numan, E. Eom, A. Li, M. Mazur, H. W. Cha, H. C. Ham, C. Jo and S.-E. Park, *ACS Catal.,* 2021, **11**, 9221-9232.
7. A. Alamdari, R. Karimzadeh and S. Abbasizadeh, *Rev. Chem. Eng.,* 2021, **37**, 481-532.
8. R. Yao, J. E. Herrera, L. Chen and Y.-H. C. Chin, *ACS Catal.,* 2020, **10**, 6952-6968.
9. Y. Pan, A. Bhowmick, W. Wu, Y. Zhang, Y. Diao, A. Zheng, C. Zhang, R. Xie, Z. Liu, J. Meng and D. Liu, *ACS Catal.,* 2021, **11**, 9970-9985.
10. P. Wang, X. Zhang, R. Shi, J. Zhao, G. I. N. Waterhouse, J. Tang and T. Zhang, *Nat. Commun.,* 2024, **15**, 789.
11. R. Zhang, H. Wang, S. Tang, C. Liu, F. Dong, H. Yue and B. Liang, *ACS Catal.,* 2018, **8**, 9280-9286.
12. L. Zhang, L. Liu, Z. Pan, R. Zhang, Z. Gao, G. Wang, K. Huang, X. Mu, F. Bai, Y. Wang, W. Zhang, Z. Cui and L. Li, *Nat. Eng.,* 2022, **7**, 1042-1051.
13. S. Song, H. Song, L. Li, S. Wang, W. Chu, K. Peng, X. Meng, Q.

Journal Name

ARTICLE

Wang, B. Deng, Q. Liu, Z. Wang, Y. Weng, H. Hu, H. Lin, T. Kako and J. Ye, *Nat. Catal.,* 2021, **4**, 1032-1042.

14. S. Shoji, X. Peng, A. Yamaguchi, R. Watanabe, C. Fukuhara, Y. Cho, T. Yamamoto, S. Matsumura, M.-W. Yu, S. Ishii, T. Fujita, H. Abe and M. Miyauchi, *Nat. Catal.,* 2020, **3**, 148-153.

15. W. Jiang, J. Low, K. Mao, D. Duan, S. Chen, W. Liu, C.-W. Pao, J. Ma, S. Sang, C. Shu, X. Zhan, Z. Qi, H. Zhang, Z. Liu, X. Wu, R. Long, L. Song and Y. Xiong, *J. Am. Chem. Soc.,* 2021, **143**, 269-278.

16. P. Wang, R. Shi, Y. Zhao, Z. Li, J. Zhao, J. Zhao, G. I. N. Waterhouse, L.-Z. Wu and T. Zhang, *Angew. Chem. Int. Ed.,* 2023, **62**, e202304301.

17. F. Niu, W. Tu, Y. Zhou, R. Xu and Z. Zou, *EnergyChem,* 2023, **5**, 100112.

18. L. Song, R. Zhang, C. Zhou, G. Shu, K. Ma and H. Yue, *Chem. Commu.,* 2023, **59**, 478-481.

19. F. Wei, W. Xue, Z. Yu, X. F. Lu, S. Wang, W. Lin and X. Wang, *Chin. Chem. Lett.,* 2024, **35**, 108313.

20. S. Bac and S. Mallikarjun Sharada, *ACS Catal.,* 2022, **12**, 2064-2076.

21. M. Zhang, G. Li, Q. Li, J. Chen, E. A. Elimian, H. Jia and H. He, *Environ. Sci. Technol.,* 2023, **57**, 4286-4297.

22. H. Zhang, S. Zuo, M. Qiu, S. Wang, Y. Zhang, J. Zhang and X. W. Lou, *Sci. Adv.,* 2020, **6**, eabb9823.

23. B. Su, Y. Kong, S. Wang, S. Zuo, W. Lin, Y. Fang, Y. Hou, G. Zhang, H. Zhang and X. Wang, *J. Am. Chem. Soc.,* 2023, **145**, 27415-27423.

24. M. Faisal, M. A. Rashed, J. Ahmed, M. Alsaiari, A. S. Alkorbi, M. Jalalah, S. A. Alsareii and F. A. Harraz, *J. Environ. Chem. Eng.,* 2021, **9**, 106773.

25. J. Peng, T. Lu, H. Ming, Z. Ding, Z. Yu, J. Zhang and Y. Hou, *Catalysts,* 2019, **9**, 1006.

26. Y. Wang, Y. Liu, L. Tan, X. Lin, Y. Fang, X. F. Lu, Y. Hou, G. Zhang and S. Wang, *J. Mater. Chem. A,* 2023, **11**, 26804.

27. R. F. Zhuo, H. T. Feng, Q. Liang, J. Z. Liu, J. T. Chen, D. Yan, J. J. Feng, H. J. Li, S. Cheng, B. S. Geng, X. Y. Xu, J. Wang, Z. G. Wu, P. X. Yan and G. H. Yue, *J. Phys. D: Appl. Phys.,* 2008, **41**, 185405.

28. A. Mezni, N. Ben Saber, M. Ibrahim, A. A. Shaltout, G. Mersal, N. Y. Mostafa, S. Alharthi, R. Boukherroub and T. Altalhi, *J. Inorg. Organomet. Polym Mater.,* 2020, **30**, 4627-4636.

29. R. C. R. Kumar, V. S. Betageri, G. Nagaraju, G. H. Pujar, H. S. Onkarappa and M. S. Latha, *J. Inorg. Organomet. Polym Mater.,* 2020, **30**, 3410-3417.

30. L. B. Chandrasekar, M. D. Gnaneswari and M. Karunakaran, *J Mater Sci-Mater El,* 2020, **31**, 20270-20276.

31. S. Sarina, H.-Y. Zhu, Q. Xiao, E. Jaatinen, J. Jia, Y. Huang, Z. Zheng and H. Wu, *Angew. Chem. Int. Ed.,* 2014, **53**, 2935-2940.

32. Z.-X. Sun, K. Sun, M.-L. Gao, O. Metin and H.-L. Jiang, *Angew. Chem. Int. Ed.,* 2022, **61**, e202206108.

33. Y. Liu, Q. Zhang, M. Xu, H. Yuan, Y. Chen, J. Zhang, K. Luo, J. Zhang and B. You, *Appl. Surf. Sci.,* 2019, **476**, 632-640.

34. Y. Zhang, M. Gao, S. Chen, H. Wang and P. Huo, *Acta Phys. -Chim. Sin.,* 2023, **39**, 2211051.

35. Z. Xiong, Y. Hou, R. Yuan, Z. Ding, W.-J. Ong and S. Wang, *Acta Phys. -Chim. Sin.,* 2022, **38**, 2111021.

36. J. Wang, Z. Wang, B. Huang, Y. Ma, Y. Liu, X. Qin, X. Zhang and Y. Dai, *ACS Appl. Mater. Interfaces,* 2012, **4**, 4024-4030.

37. X. Wang, L. Zhao, X. Li, Y. Liu, Y. Wang, Q. Yao, J. Xie, Q. Xue, Z. Yan, X. Yuan and W. Xing, *Nat. Commun.,* 2022, **13**, 1596.

38. C. Zhang, Y. Hao, X. Wang, D. Hu, N. Sun and W. Wei, *Catal. Sci. Technol.,* 2024, **14**, 935-944.

39. R. Wang, P. Yang, S. Wang and X. Wang, *J. Catal.,* 2021, **402**, 166-176.

40. G. Chen, F. Wei, Z. Zhou, B. Su, C. Yang, X. F. Lu, S. Wang and X. Wang, *Sustainable Energy Fuels,* 2023, **7**, 381-388.

41. R. Huang, O. Kwon, C. Lin and R. J. Gorte, *J. Catal.,* 2021, **398**, 102-108.

42. H. Tang, Y. Su, Y. Guo, L. Zhang, T. Li, K. Zang, F. Liu, L. Li, J. Luo, B. Qiao and J. Wang, *Chem. Sci.,* 2018, **9**, 6679-6684.

43. F. Wang, S. He, H. Chen, B. Wang, L. Zheng, M. Wei, D. G. Evans and X. Duan, *J. Am. Chem. Soc.,* 2016, **138**, 6298-6305.

44. M. Xu, S. Yao, D. Rao, Y. Niu, N. Liu, M. Peng, P. Zhai, Y. Man, L. Zheng, B. Wang, B. Zhang, D. Ma and M. Wei, *J. Am. Chem. Soc.,* 2018, **140**, 11241-11251.

45. X. Ge, M. Dou, Y. Cao, L. Xi, Y. Qiang, Z. Jing, Q. Gang, X. Gong, X. Zhou, L. Chen, W. Yuan and X. Duan, *Nat. Commun.,* 2022, **13**, 5534.

46. Q. Guan, J. Zhang, L. He, R. Miao, Y. Shi and P. Ning, *ACS Sustain. Chem. Eng.,* 2020, **8**, 11638-11648.

47. T. Yang, M. Zhao, X. Wang, R. Ma, Y. Liu, Y. He and D. Li, *Catal. Lett.,* 2022, **152**, 227-238.

48. X. Weng, X. Yuan, H. Li, X. Li, M. Chen and H. Wan, *Sci. China Chem.,* 2015, **58**, 174-179.

49. X. Han, W. Feng, X. Chu, H. Chu, L. Niu and G. Bai, *J. Nanopart. Res.,* 2017, **19**, 79.

50. S. Wang, Y. Wang, S. L. Zhang, S.-Q. Zang and X. W. Lou, *Adv. Mater.,* 2019, **31**, 1903404.

51. J.-C. Wang, X. Qiao, W. Shi, J. He, J. Chen and W. Zhang, *Acta Phys. -Chim. Sin.,* 2023, **39**, 2210003.

52. H. Li, H. Gong and Z. Jin, *Acta Phys. -Chim. Sin.,* 2022, **38**, 2201037.

53. S. Wang, B. Y. Guan, X. Wang and X. W. Lou, *J. Am. Chem. Soc.,* 2018, **140**, 15145-15148.

54. B. Su, M. Zheng, W. Lin, X. F. Lu, D. Luan, S. Wang and X. W. Lou, *Adv. Eng. Mater.,* 2023, **13**, 2203290.

55. H. Yang, M. Zhang, Z. Guan and J. Yang, *Catal. Sci. Technol.,* 2023, **13**, 6238-6246.

56. W. Tu, Y. Yang, C. Chen, T. Zhou, T. Li, H. Wang, S. Wu, Y. Zhou, D. O'Hare, Z. Zou and R. Xu, *Small Struct.,* 2023, **4**, 2200233.

57. F. Guo, B. Hu, C. Yang, J. Zhang, Y. Hou and X. Wang, *Adv. Mater.,* 2021, **33**, 2101466.

58. B. Su, L. Huang, Z. Xiong, Y. Yang, Y. Hou, Z. Ding and S. Wang, *J. Mater. Chem. A,* 2019, **7**, 26877-26883.

59. Y. Tang, J. Qiu, D. Dai, G. Xia, L. Zhang and J. Yao, *Catal. Sci. Technol.,* 2024, **14**, 83-89.

60. H. Wu, L. Lai, Z. Li, J. Hu, L. Zhang, W. Younas and Q. Liu, *Catal. Sci. Technol.,* 2023, **13**, 6635-6639.

61. Y. Tang, M. Chen, C. Zhang, H. Li, Y. He, X. Lai, L. Tao, J. Jing and X. Liu, *Catal. Sci. Technol.,* 2023, **13**, 5326-5332.

62. C. He, S. Wu, Q. Li, M. Li, J. Li, L. Wang and J. Zhang, *Chem,* 2023, **9**, 3224-3244.

63. J. Xie, Y. Jiang, S. Li, P. Xu, Q. Zheng, X. Fan, H. Peng and Z. Tang, *Acta Phys. -Chim. Sin.,* 2023, **39**, 2306037.

64. L. Wang, B. Zhao, C. Wang, M. Sun, Y. Yu and B. Zhang, *J. Mater. Chem. A,* 2020, **8**, 10175-10179.